Planetary Rotation Effects on Ionospheric Electrodynamics with Closed-Field, Magnetospherically Unforced Polar Caps: Earth-Parameterized Simulations with Implications for Jupiter and Saturn

Junjie Chen[1*], Jiuhou Lei[2], Peter A. Delamere[3], and Binzheng Zhang[1*]

[1]Department of Earth and Planetary Sciences, The University of Hong Kong, Pokfulam, Hong Kong SAR, China

[2]School of Earth and Space Sciences, University of Science and Technology of China, Hefei, China

[3]Geophysical Institute, University of Alaska Fairbanks, Fairbanks, AK, USA

Correspondence to: Junjie Chen (cjjvince@hku.hk) and Binzheng Zhang (binzh@hku.hk)

Key Points:

- Simulations predict that ionospheric convection transitions from two-cell to one-cell patterns in magnetospherically unforced polar caps.
- The one-cell pattern is driven by the wind dynamo, governed by the pressure gradient from neutral temperatures and the Coriolis force.
- The efficiency of the polar wind dynamo is suppressed by faster planetary rotation due to Coriolis-induced deceleration of neutral winds.

Abstract

Ionospheric electrodynamics are classically governed by magnetic topology, with solar wind driving two-cell convection in open polar regions and neutral wind dynamo prevailing at closed lower latitudes. However, it remains unclear whether this paradigm applies to fast-rotating planets or Earth's state with extremely weak upstream conditions, where polar regions become largely closed. Global Earth-based simulations under closed-field, magnetospherically unforced polar cap conditions predict that the neutral wind dynamo generates a one-cell convection pattern in polar regions, a fundamental departure from the magnetospherically-driven two-cell structure. The convection direction is primarily controlled by the pressure gradient from neutral temperature distributions and the Coriolis force, forming counterclockwise flow around high-latitude cold regions and clockwise around low-latitude warm regions in the Northern Hemisphere. Furthermore, faster planetary rotation suppresses dynamo efficiency through Coriolis-induced wind deceleration. These results establish a theoretical baseline for planetary atmospheric ion-neutral coupling without imposed magnetospheric forcing.

Plain Language Summary

The movement of charged particles in planetary upper atmospheres, known as ionospheric electrodynamics, is usually shaped by planetary magnetic field and its interactions with the solar wind. At Earth, polar regions are typically open to the solar wind, which strongly influences the ionospheric behavior. However, for distant and fast-rotating giant planets like Jupiter or Saturn, recent research suggests their polar regions may be mostly magnetically closed, making internal atmospheric processes more important. However, how these internal processes control the polar dynamics under such conditions remains an open question. In this study, we use numerical simulations based on Earth-like conditions to explore what happens when the polar regions are magnetically closed, magnetospherically unforced, and the planet's rotation rate varies. Our results show that the typical two-cell flow pattern changes to a single circulation cell in the polar ionosphere. This pattern is driven by winds in the neutral atmosphere, influenced by temperature differences and the planet's rotation. We also find that as the planet spins faster, the efficiency of these internal winds in driving the ionospheric currents decreases. These findings provide a theoretical baseline for interpreting internal electrodynamics of rapidly rotating giant planets and for Earth under extremely weak solar wind conditions.

1. Introduction

Ionospheric electrodynamics, governing electric field generation and charged particle motion, modulate energy and momentum transfer between the solar wind, magnetosphere, and upper atmosphere in planetary space environments (Richmond & Thayer, 2000; Schunk & Nagy, 2000; Kelley, 2009). The canonical paradigm, established from rich datasets at Earth, distinguishes distinct electrodynamic regimes according to magnetic field topology (Heelis, 2004; Kivelson & Ridley, 2008). Electrodynamics at high latitudes with open and magnetotail-connected closed field lines are dynamically controlled by solar wind-magnetosphere interactions (Dungey, 1961; Cowley & Lockwood, 1992). The upstream solar wind typically forces ionospheric plasma to convect according to a characteristic two-cell pattern, featuring antisunward flow over the polar cap and return flow at lower (60-75°) magnetic latitudes (MLATs) under southward interplanetary magnetic field (IMF) conditions, while more complex structures may occur under other IMF orientations (Rasmussen & Schunk, 1987; Crooker & Rich, 1993; Reiff & Heelis, 1994; Ruohoniemi & Greenwald, 2005; Lu et al., 2011). At middle and low (below ~60°) latitudes, magnetic field lines are topologically closed, connecting conjugate ionospheres, and the ionosphere is largely shielded from direct solar wind forcing. Here, the neutral wind dynamo, mainly powered by solar irradiation, becomes the primary driver of electric fields and currents during geomagnetically quiet conditions, while penetration electric fields from high latitudes become increasingly significant during enhanced upstream conditions (Richmond, 1995b; Rishbeth, 1997).

However, observations from gas giants imply that the Earth-based paradigm may not directly apply to such rapidly rotating systems due to fundamentally different dominant energy sources and magnetospheric topology. At Jupiter and Saturn, powerful auroral emissions and strong high-latitude particle heating attest to intense magnetospheric energy deposition (Cowley & Bunce, 2001; Bunce et al., 2008; O'Donoghue et al., 2021). These energies largely originate from internally powered magnetospheres, driven by planetary rotation and moon-related mass loading (Hill, 1979; Khurana et al., 2004; McComas & Bagenal, 2007, 2008), with additional contributions from solar wind interaction and reconnection (Gurnett et al., 2002; Cowley et al., 2003; Cowley et al., 2004; Crary et al., 2005). Recent observational analyses, along with numerical simulations, suggest that their polar cap, particularly at Jupiter, could be largely closed magnetic field lines, effectively forming vast, closed magnetospheric lobe regions (Zhang et al., 2021; Szalay et al., 2022; Chen et al., 2023; Zhang et al., 2024). Such a magnetically closed topology, together with existing voltage estimates (Badman & Cowley, 2007) and studies of viscous-like magnetopause interactions (Delamere & Bagenal, 2010, 2013), suggests that the polar ionosphere may be largely decoupled from direct Dungey-cycle solar wind driving. Dungey- and Vasyliunas-cycle contributions may nevertheless overlap and remain difficult to distinguish from the ionospheric flow pattern alone (Badman & Cowley, 2007). Infrared H_3^+ observations and related auroral studies also reveal structured and variable high-latitude dynamics at giant planets (see Stallard et al., 2012, and references therein), including sub-corotation associated with Saturn's Enceladus torus and localized corotation poleward of the main auroral oval (Stallard et al., 2007a; Stallard et al., 2007b), as well as Jovian sub-corotation, near-corotation, dawnside stagnation or possible return flows, and asymmetric auroral jets (Rego et al., 1999; Stallard et al., 2001; Stallard et al., 2003; Johnson et al., 2017; R. Wang et al., 2023).

In closed or weakly solar-wind-forced polar regions, ionospheric electrodynamics may be affected by two broad classes of internally related processes. One is direct magnetosphere-ionosphere electrodynamic forcing, in which internally-driven magnetospheric dynamics generate field-aligned currents and closure currents that impose ionospheric electric potentials and drive $E \times B$ convection. Such forcing is important in rapidly rotating, internally mass-loaded systems and is central to conventional interpretations of giant-planet auroral electrodynamics (Hill, 1979; Cowley & Bunce, 2001; Cowley et al., 2003; Nichols, 2011). The other is a thermosphere-ionosphere dynamo pathway, in which thermospheric heating from auroral precipitation, Joule heating, and solar irradiance, together with ion drag, and rotational/Coriolis effects, shapes thermospheric temperature, pressure gradients, neutral winds, and ionospheric conductivity. These neutral winds can then generate dynamo electric fields through ion-neutral coupling (Richmond, 1995b; Rishbeth, 1997; Richmond & Thayer, 2000; Millward et al., 2005; Chen & Lei, 2019). Terrestrial studies reveal that the wind dynamo can generate significant electrical energy, although in high-latitude terrestrial conditions neutral winds are ultimately strongly driven by magnetospheric energy input (Thayer & Vickrey, 1992). This suggests that internal atmospheric ion-neutral coupling could modify convection if the background horizontal wind is strong enough. In real giant-planet ionospheres, the magnetosphere-ionosphere coupling and wind-dynamo pathways are coupled, leaving the stand-alone wind-dynamo contribution difficult to isolate. Direct observations of both ionospheric and thermospheric winds within the same relatively high layer of Jupiter's upper atmosphere highlight the importance of asymmetric winds in this region (R. Wang et al., 2023). However, these observations do not directly constrain the relative balance between magnetosphere–ionosphere coupling and wind-dynamo forcing within the underlying Pedersen-conducting layer.

To isolate this internal wind-dynamo contribution, we investigate the theoretical limiting case with closed-field, magnetospherically unforced polar-cap conditions. Using global simulations with Earth-based planetary parameters, we impose magnetically closed polar cap conditions and systematically change the planetary Coriolis forcing. This approach addresses a foundational question: what convection pattern emerges from the stand-alone neutral wind dynamo, and how is it governed by planetary rotation and the neutral atmosphere structure?

2. Methods

We conducted our numerical experiments using the Thermosphere–Ionosphere–Electrodynamics General Circulation Model (TIEGCM) (Roble et al., 1988; Richmond et al., 1992). The model solves the nonlinear equations of continuity, energy, and momentum for neutral and ion species, and self-consistently computes ionospheric electrodynamics under a specified geomagnetic field configuration (Richmond & Maute, 2014). All simulations retain the standard terrestrial composition and chemistry, with N_2, O_2, and O as the dominant neutral constituents, and O^+, O_2^+, and NO^+ as the principal ion species relevant to ionospheric electrodynamics. It was configured with a horizontal resolution of 2.5° × 2.5° and a vertical resolution of 1/4 scale height, spanning from 97 km to 450–700 km depending on solar activity. All simulations use an Earth-like, axisymmetric, non-offset dipole magnetic field with the magnetic axis aligned with the planetary rotation axis. They are run under quiet geomagnetic conditions (Kp = 1), with solar irradiance for moderate activity (F10.7 = 100 sfu) at the vernal equinox. We conduct two sets of rotation-rate experiments, one without lower-atmospheric tidal forcing and one with migrating diurnal and semidiurnal tides imposed at the lower boundary from the Global Scale Wave Model (GSWM; Hagan & Forbes, 2002, 2003). GSWM is a two-dimensional, linearized, steady-state model based on prescribed terrestrial background climatologies, and the same GSWM-derived tidal forcing is imposed across all tide-forced cases.

In the standard model setup, high-latitude electrodynamics are driven by a combination of internal and external processes. At magnetic latitudes below ~60°, the electric potential is determined primarily by the neutral wind dynamo (Richmond et al., 1992) and by penetration electric fields from high-latitude magnetospheric convection (Foster & Rich, 1998; W. Wang et al., 2008b). At magnetic latitudes above ~75°, it is specified by the empirical Heelis model (Heelis et al., 1982), which imposes a cross-polar cap potential (CPCP) indexed by Kp. These solutions are blended linearly in the transition region (~60°–75°), producing the canonical two-cell convection pattern under open field line conditions (Richmond, 1995a; Heelis, 2004).

To investigate ionospheric electrodynamics under closed-field, magnetospherically unforced polar-cap conditions, we removed prescribed external driving from solar wind-magnetosphere interactions by disabling the high-latitude electric potential, field-aligned currents and auroral particle precipitation from the empirical model. Field-aligned currents associated with the self-consistent ionospheric electrodynamic solution are allowed to flow between conjugate ionospheric foot points, as in the Richmond and Roble (1987) treatment. In this idealized configuration, the high-latitude electric potential is generated self-consistently by the neutral wind dynamo alone.

The TIEGCM equations are solved in a planet-fixed geographic coordinate system, and neutral winds are calculated as velocities relative to this rotating frame. We systematically conducted idealized Coriolis-scaling experiments by multiplying the Coriolis parameter from 1.0 to 2.4, 10, 24, and 100 times the terrestrial value while holding all other parameters constant. This scaling was applied uniformly at all model pressure levels. No altitude-dependent angular velocity, differential rotation, or prescribed atmospheric spin-up was imposed. The neutral winds at different altitudes are instead calculated self-consistently by the model. This sequence was designed to span a wide parameter range, covering Earth-like conditions to those far exceeding known gas giants. The scaling factors approximately represent combinations of rotation rate (e.g., ~2.4 for Jupiter/Earth ratio) and planetary size/magnetic field (e.g., ~10). The approach is inspired by the transition in magnetospheric morphology from terrestrial to gas giant regimes (Zhang et al., 2024), though the underlying ionospheric physics may differ. Note that this approach intentionally does not alter the fixed 24-hour solar irradiation cycle and the Earth-like lower-boundary tidal conditions, in order to focus directly upon the electrodynamic response to changes in the Coriolis force. A shorter solar day would also modify thermospheric heating, ionospheric photochemistry, and atmospheric tides. Thus, these simulations should be interpreted as controlled experiments rather than fully self-consistent models of gas-giant differential rotation, rotation-dependent tides, or deep-atmosphere coupling.

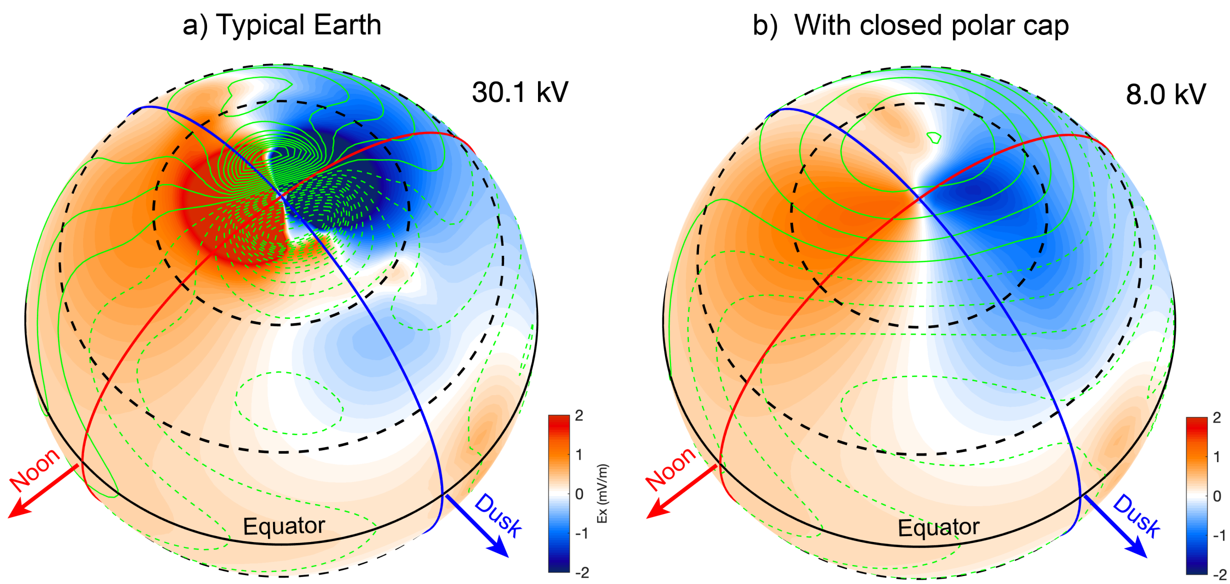

Figure 1. Simulated ionospheric electric fields in the Northern Hemisphere under different magnetic configurations. (a) Standard Earth's run with dipole magnetic fields during geomagnetically quiet (Kp = 1.0) and moderate solar activity ($F_{10.7}$ = 100) conditions. (b) The closed-cap, magnetospherically unforced baseline run: idealized configuration with a fully closed polar cap and no magnetosphere/solar wind inputs. The color shading represents the zonal electric field (positive eastward), and the overlaid contour lines denote the electrostatic potential (interval = 1 kV). Solid and dashed contours indicate positive and negative potentials, respectively.

3. Results

Figure 1a presents the electric field simulated by the standard Earth run with geomagnetically quiet (Kp = 1.0) and moderate solar activity ($F_{10.7}$ = 100) conditions. Zonal electric fields (color shading) exhibit a diurnal variation, with eastward (positive) fields dominating on the dayside and westward (negative) fields on the nightside, featuring a pre-reversal enhancement of 0.59 mV/m near the equatorial dusk terminator. While the mid- and low-latitude (<60° MLAT) zonal electric field remains below 1.13 mV/m, driven primarily by the neutral wind dynamo and modulated by penetration electric fields, the high-latitude region (> 60°) shows significantly stronger electric fields, peaking at 16.84 mV/m on the dayside and -17.27 mV/m on the nightside, which are imposed by magnetospheric convection. The electrostatic potential (contour lines) reveals a characteristic two-cell structure. Positive potentials (solid contours) are located in the dawn hemisphere, while negative potentials (dashed contours) dominate in the dusk hemisphere. The total CPCP difference is 30.1 kV. The horizontal components of the plasma $E \times B$ drift are parallel to these potential contours. Consequently, the flow forms an antisunward motion across the polar cap and a return sunward flow at lower latitudes, encircling the positive (counterclockwise) and negative (clockwise) potential cells. This pattern is the hallmark two-cell convection typically observed under southward IMF conditions, driven by the solar wind-magnetosphere interaction (Dungey, 1961; Cowley & Lockwood, 1992).

Figure 1b displays the electrodynamic state in the closed-field, magnetospherically unforced baseline run, in which direct magnetospheric and solar wind forcing have been removed. The mid- and low-latitude electric fields remain nearly identical in structure and amplitude (≤1.13 mV/m) to the standard run (Figure 1a), indicating that these regions are indeed dominated by the internal neutral wind dynamo and are not largely affected by the removal of magnetospheric drivers. In contrast, the global magnitude of the high-latitude electric field is drastically reduced, with peaks diminishing to 1.23 mV/m on the dayside and -1.45 mV/m on the nightside (Figure 1b), an order of magnitude lower than the values of 16.84 and -17.27 mV/m in the standard run (Figure 1a). This electric field distribution sustains a morphologically distinct convection pattern where the characteristic two-cell structure is entirely replaced by a single cell in polar regions. The corresponding CPCP drops to 8.0 kV, a ~70% reduction from the standard run. This potential distribution is comparable with respect to previous ideal studies (Richmond & Roble, 1987).

The stark contrast between Figures 1a and 1b within the polar auroral region underscores that the magnetospherically-imposed convection dominates high-latitude electrodynamics even during quiet conditions (Kp=1.0), justifying the conventional attribution of polar convection to magnetospheric driving. However, this attribution should not be misconstrued as the neutral wind dynamo being electrodynamically insignificant. Intense high-latitude thermospheric winds (often 100–150 m/s), generated in response to magnetospheric energy deposition via ion drag and Joule heating (W. Wang et al., 2008a; Tan et al., 2022), can store substantial mechanical energy. Diagnostic studies suggest that these winds alone can generate an electrical energy flux comparable to that from the direct magnetospheric dynamo (e.g., reaching ~8 mW/m² from winds versus ~12 mW/m² from magnetospheric driving; Thayer & Vickrey, 1992). However, in typical coupled models, these wind-driven electric fields are inherently aligned with and embedded within the magnetospherically-driven convection pattern. Therefore, from an energy partitioning perspective, there is little need to treat them separately, and current empirical models (Heelis et al., 1982; Weimer, 2005) effectively capture their contribution as part of the net magnetospheric forcing. Our experiment in Figure 1b deliberately steps outside this coupled framework to investigate the wind dynamo in isolation. By removing the dominant magnetospheric driver, we can answer a fundamental question: what is the intrinsic structure of polar convection when it is generated self-consistently by the neutral wind dynamo alone? The following analysis will characterize this emergent one-cell pattern and quantify its dependence on the planetary rotation and solar irradiation, which control the Coriolis force and the global neutral temperature structure that govern thermospheric winds and thus the wind dynamo.

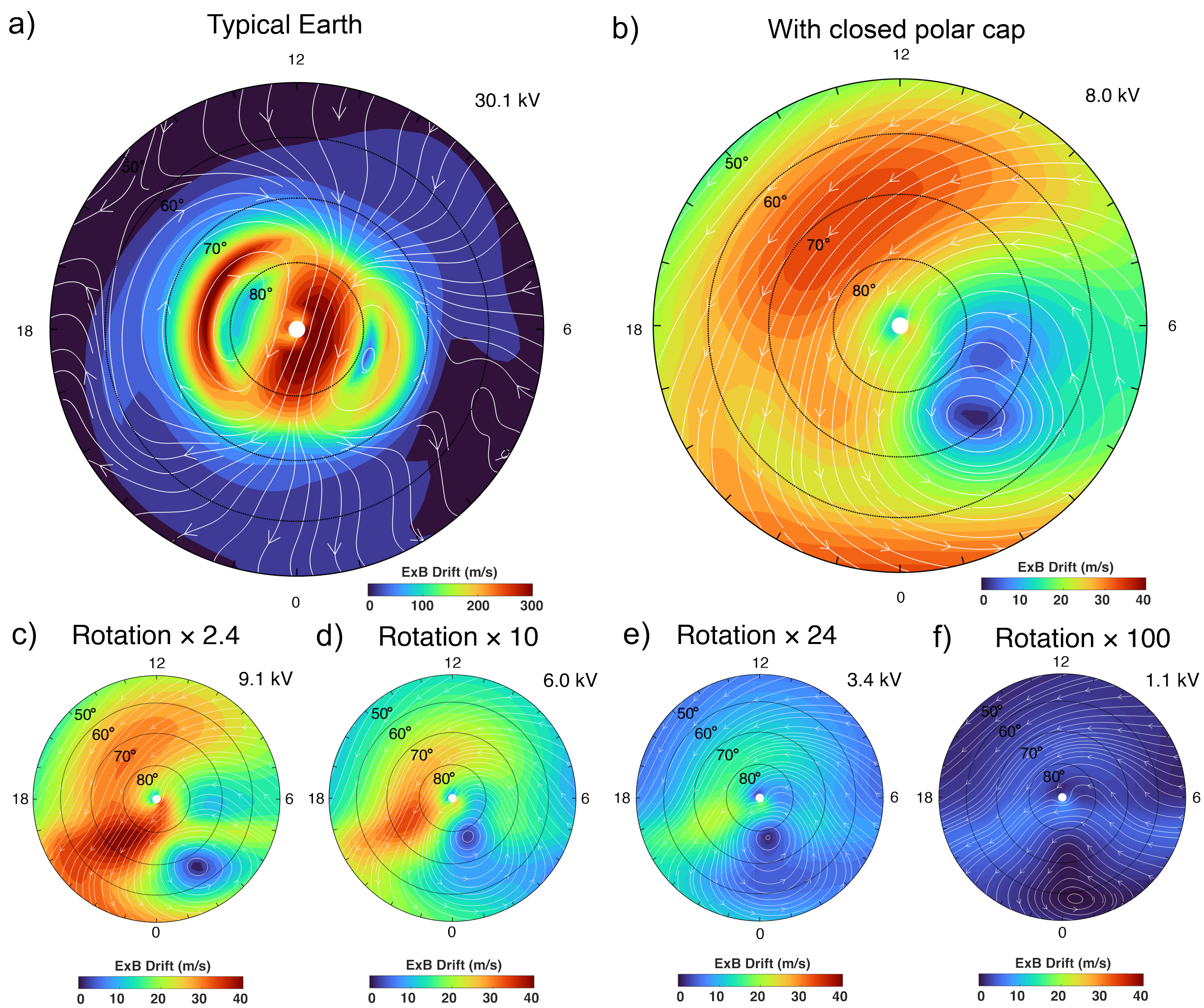

Figure 2. Dependence of simulated ionospheric convection patterns in the Northern Hemisphere on planetary rotation with closed polar cap. (a) Standard Earth run with dipole magnetic fields during geomagnetically quiet (Kp = 1.0) and moderate solar activity ($F_{10.7}$ = 100) conditions. (b) Closed-cap, magnetospherically unforced baseline run: idealized configuration with a fully closed polar cap and no magnetospheric or solar wind forcing. (c–f) Closed-cap runs with the Coriolis parameter scaled to 2.4, 10, 24, and 100 times the terrestrial value, respectively. The color shading and arrows represent the magnitude and direction of $E \times B$ drifts, respectively.

Figure 2 shows the systematic changes in high-latitude convection resulting from variations in planetary rotation under magnetically closed polar caps. The standard run (Figure 2a) reproduces the classic two-cell pattern with antisunward flow over the polar cap and return sunward flow at lower latitudes, where $E \times B$ drift velocities exceed 300 m/s. In contrast, the closed-cap baseline run (Figure 2b), without imposed magnetospheric forcing, exhibits a single-cell pattern around ~70° and 3 MLT, with a markedly weaker peak drift of ~40 m/s and an overall dawn-to-dusk flow across the polar cap.

As the Coriolis parameter increases from 1.0 to 100 times the terrestrial value, the one-cell structure persists but undergoes significant morphological and intensity changes (Figures 2b–f). The cell center, distinct from the closed-cap baseline run and the slow 2.4-time rotation run, progressively shifts toward midnight (0 MLT) at intermediate rotation rates (10 and 24 times) and subsequently moves to lower latitudes (~55°) at the extreme 100-time rotation. Concurrently, the convection strength exhibits a non-monotonic response: it slightly intensifies at 2.4-time rotation but then declines at higher rates. This suppression is quantitatively underscored by the CPCP, which peaks at 9.1 kV for the 2.4-time-rotation run before falling to 6.0, 3.4, and 1.1 kV for the 10-time, 24-time, and 100-time runs, respectively. This clear damping of both the flow velocity and the CPCP with increasing rotation beyond a threshold (~2.4 times) demonstrates a substantial suppression of the neutral wind dynamo efficiency, governed primarily by the strengthening Coriolis force.

To examine the mechanisms governing the one-cell convection structure and the response of the dynamo efficiency to the Coriolis force across our closed runs, we analyze the two end-member scenarios: the 2.4-time-rotation run (strongest convection) and the 100-time-rotation run (weakest convection). Figure 3 presents the E-region $E \times B$ drifts, neutral winds, and neutral temperature across the Northern Hemisphere for these two runs.

In the 2.4-time-rotation run (Figures 3a–c), the $E \times B$ drift (Figure 3a) exhibits a large-scale clockwise flow at low latitudes on the dayside afternoon and a distinct counterclockwise cell centered near 75° MLAT and 3:00 MLT. This pattern closely mirrors the structure of the horizontal neutral wind (Figure 3b), particularly the large-scale clockwise circulation on the dayside, which is expected as the dayside electrodynamics are primarily driven by the E-region dynamo. On the nightside, the neutral wind also shows a counterclockwise circulation, centered near 85° MLAT and 5:00 MLT, albeit with a slight offset from the $E \times B$ drift cell. This offset likely arises because the nightside Pedersen conductivity peak lies in the F-region, and the electric field must adjust to maintain a large-scale conservative pattern in response to the dayside dynamo. Overall, the large-scale $E \times B$ drift circulation corresponds to the horizontal neutral wind distribution. The neutral wind structure, in turn, corresponds to the neutral temperature (T_n, Figure 3c) distribution, which is associated with neutral pressure distribution. A temperature maximum is located near 30° MLAT and 15 MLT, while a minimum is found around 80° MLAT and 6:00 MLT. The neutral temperature contours exhibit a notable similarity to the wind flow pattern, indicative of a wind field primarily governed by a balance between the pressure gradient force associated with neutral temperature distribution and the Coriolis force, yielding characteristics analogous to geostrophic flow in the lower atmosphere (Tarbuck & Lutgens, 1979).

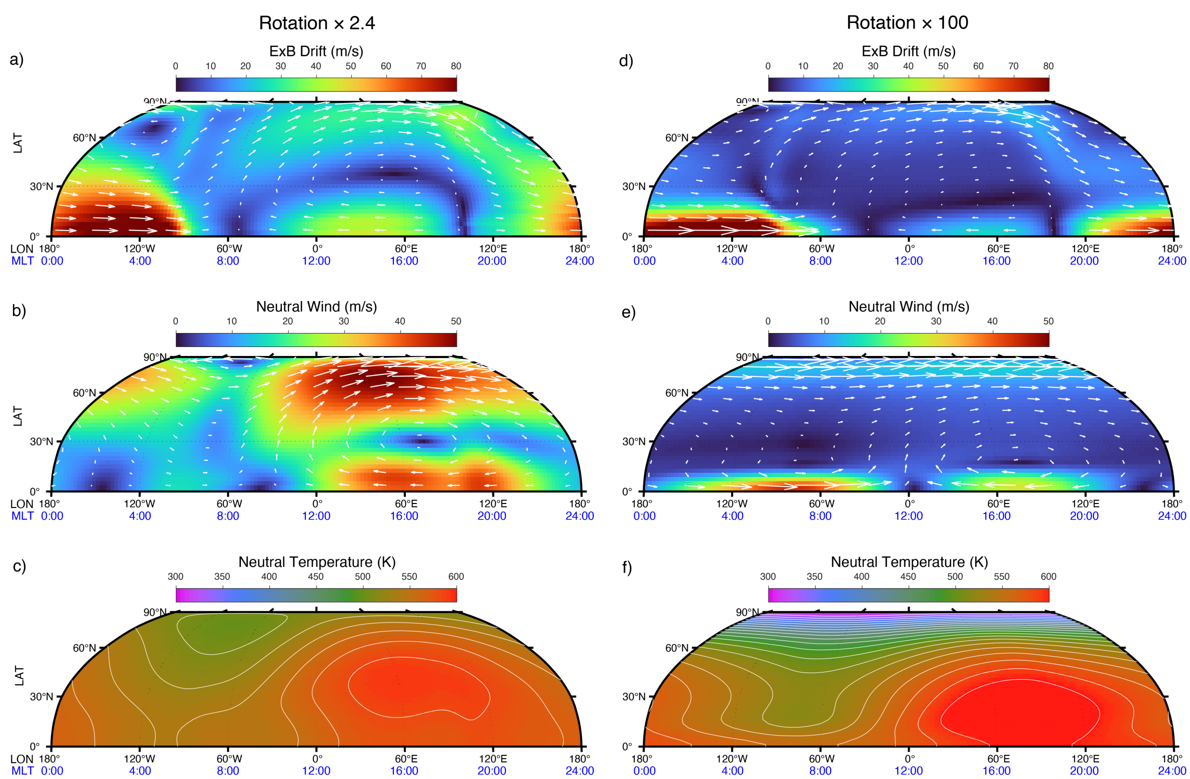

Figure 3. Simulated E-region ionosphere-thermosphere parameters under different Coriolis parameters for the closed polar cap and magnetospherically unforced scenario. The left column (a-c) corresponds to the run with a Coriolis parameter 2.4 times the terrestrial value, and the right column (d-f) corresponds to 100 times the terrestrial value. (a, d) Horizontal $E \times B$ drift velocity (color shading) with overlaid flow vectors (arrows). (b, e) Horizontal neutral wind velocity (color shading) with overlaid wind

flow vectors (arrows). (c, f) Neutral temperature (color shading). The contour lines are overlaid at intervals of 15 K. The simulations show that the stronger Coriolis force in the faster-rotating run (right column) significantly reorganizes the flow patterns and suppresses the dynamo efficiency. All results are at the pressure level Z_P = -4 (approximately ~130 km, near the daytime E-region Pedersen conductivity peak).

In the 100-time-rotation run (right panels of Figure 3), the $E \times B$ convection pattern (Figure 3d) is not simply a uniformly weakened version of the 2.4-time-rotation case, but is reorganized into a weaker and more symmetric structure. A dawnside poleward drift of order ~10 m/s remains over a broad latitude range, whereas the duskside equatorward branch is reduced from ~30-40 m/s in the 2.4-time run (Figure 3a) to ~10 m/s in the 100-time run (Figure 3d). Thus, the main change is not only a reduction in drift magnitude but also a transition from the more displaced and asymmetric circulation to a more symmetric large-scale pattern. This behavior reflects the fact that the $E \times B$ drift is determined by the electrostatic potential obtained from the global, conductivity-weighted wind-dynamo current-closure problem, rather than by the local neutral wind alone. A related reorganization is also seen in the neutral wind distribution (Figure 3e). Under very strong Coriolis forcing, the meridional neutral wind is strongly suppressed and the wind field becomes increasingly dominated by zonal components, with westward winds between 12–20 MLT and eastward winds during other MLTs at low latitudes. This change in the neutral wind geometry reorganizes the wind-dynamo source term and redistributes the electric potential, thereby weakening the duskside return branch while maintaining a weaker dawnside poleward branch. Furthermore, the neutral temperature distribution is substantially altered. Figures 3c and 3f show that the low-latitude temperature in the 100-time run is slightly higher (~600 K) than in the 2.4-time run (~570 K). In contrast, the high-latitude temperature (~300 K) is significantly colder than its 2.4-time counterpart (~450–500 K). This enhanced latitudinal temperature gradient arises because a stronger Coriolis force requires weaker wind speeds to balance a given pressure gradient force. As solar radiation primarily heats low-to-mid latitudes, the reduced wind-driven advection inhibits efficient heat redistribution to high latitudes, thereby amplifying the temperature contrast. The thermospheric momentum balance also includes ion drag, viscosity, nonlinear advection, and other forcing terms besides the pressure-gradient and Coriolis forces (Roble et al., 1988; Richmond et al., 1992; Richmond & Thayer, 2000). As the Coriolis scaling increases, the system tends toward a more geostrophic-like balance, in which enhanced pressure gradients can be balanced by weaker horizontal winds, thereby suppressing the wind dynamo efficiency.

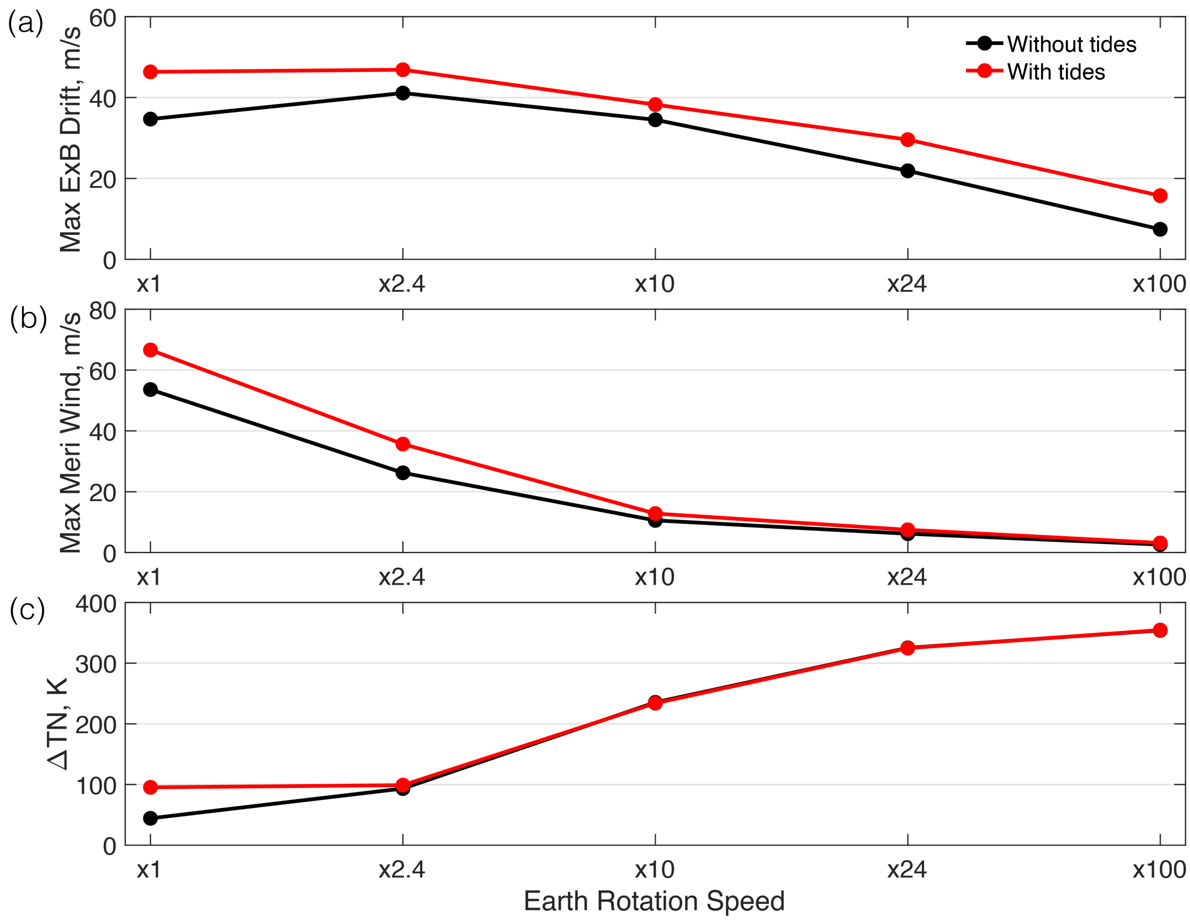

Figure 4. Sensitivity of the closed-polar-cap simulations to lower-boundary tidal forcing as a function of the imposed Coriolis scaling factor. (a) Peak horizontal $E \times B$ drift speed poleward of 50° magnetic latitude. (b) Peak absolute meridional neutral wind speed. (c) Maximum difference in E-region neutral temperature. Black curves correspond to simulations without lower-boundary tides, and red curves correspond to simulations including migrating diurnal and semidiurnal tides from the Global Scale Wave Model (GSWM). The horizontal axis denotes the Coriolis scaling factor relative to the terrestrial value. All diagnostics are evaluated at Z_P = -4, approximately 130 km, near the daytime E-region Pedersen conductivity peak.

Figure 4 summarizes how the wind-dynamo response varies with imposed rotation rate and lower-boundary tidal forcing. This comparison is motivated by classical terrestrial wind-dynamo studies, in which lower-atmospheric tides can substantially amplify electrodynamic variations (Richmond & Roble, 1987; Richmond, 1995b). In our simulations, increasing the Coriolis scaling reduces both high-latitude horizontal $E \times B$ drift and the peak meridional neutral wind, while increasing the E-region neutral temperature contrast. Within the present configuration, this suggests that faster rotation inhibits meridional heat redistribution and helps maintain stronger temperature gradients, but also weakens the meridional wind response that drives the wind dynamo. Adding the prescribed empirical migrating diurnal and semidiurnal tides (Hagan & Forbes, 2002, 2003) modifies the amplitudes of the simulated drifts and winds, generally enhancing them, but does not alter the rotation-dependent trend in these sensitivity tests. Because the same Earth-based tidal perturbations are imposed for all rotation rates, rather than being recalculated self-consistently for each rotation state, these simulations should be interpreted as a sensitivity test of lower-boundary forcing rather than as a complete treatment of rotation-dependent tidal effects. A full heat-budget diagnosis would be required to determine how rotation changes the balance between horizontal energy redistribution by meridional winds and vertical transport by diffusion, waves, and tides. This distinction is relevant to future applications to rapidly rotating planetary thermospheres, where the partition between horizontal redistribution and vertical transport remains an important open problem.

4. Discussion

Our simulations demonstrate that under magnetically closed and magnetospherically unforced polar cap conditions, high-latitude ionospheric convection can be generated by the neutral wind dynamo and organizes into a one-cell pattern rather than the usual solar-wind-driven two-cell pattern. The pattern's intensity and detailed morphology evolve with rotation rate, but its direction remains closely tied to the pressure gradient associated with neutral temperature distribution. In the Northern Hemisphere, the simulated $E \times B$ flows consistently exhibit counterclockwise circulation around nightside, high-latitude cold regions and clockwise circulation around the dayside, lower-latitude warm region. This relationship arises from the neutral wind direction dominated by the pressure gradient force and the Coriolis force, analogous to cyclonic and anticyclonic flow in the troposphere (Tarbuck & Lutgens, 1979). These thermospheric winds then drive electric fields by the wind dynamo and further cause the corresponding convective $E \times B$ drift. As the imposed rotation rate increases, the neutral temperature contrast becomes larger, but the meridional neutral wind and $E \times B$ drift become weaker. This interpretation is consistent with the established theory of wind dynamo-driven convection at middle and low latitudes (e.g., Richmond, 1995b) and with earlier idealized studies showing that thermospheric winds can drive ionospheric electric fields even without imposed magnetospheric forcing (Richmond & Roble, 1987).

The rotation-dependent changes in thermal structure and neutral winds provide a qualitative reference for rapidly rotating planetary ionospheres with closed and weakly forced polar caps. Figures 3c, 3f, and 4c indicate that stronger Coriolis forcing reduces horizontal redistribution of thermospheric energy in our solar-radiation-driven case. Because early Earth rotated more rapidly than today (Green et al., 2017; Mitchell & Kirscher, 2023), the non-monotonic Coriolis response found here suggests that faster rotation could have altered thermospheric heat redistribution and the resulting wind-dynamo convection, although its magnitude would depend on contemporaneous solar and atmospheric conditions. In real gas-giant auroral regions, however, the high-latitude thermal and electrodynamic structures are dominated by magnetosphere-ionosphere coupling. At Jupiter, enhanced H_3^+ temperatures have been observed in and poleward of the main auroral oval (O'Donoghue et al., 2021), although comparisons with neutral temperatures require caution, since H_3^+ traces the neutral gas only under quasi-local thermodynamic equilibrium (LTE) conditions and non-LTE effects may occur at higher altitudes (Tao et al., 2011; Giles et al., 2016). Such auroral heating may modify neutral temperatures and winds by analogy with terrestrial auroral heating (Xu et al., 2013). In addition, Jovian and Kronian auroral electrodynamics are strongly controlled by current closure and coupling to rapidly rotating magnetospheric plasma (Hill, 1979; Cowley & Bunce, 2001; Nichols, 2011; Stallard et al., 2012), and observations show structured ion and neutral flows, including sub- and super-corotational motion, possible return flows, asymmetric jets, and ion-neutral relative motion (Chaufray et al., 2011; Johnson et al., 2017; Cavalié et al., 2021; R. Wang et al., 2023). Recent observations of Jupiter's UV-dark polar ovals further suggest that magnetospheric forcing may organize large-scale polar atmospheric structures and potentially influence atmospheric dynamics down to stratospheric levels (Tsubota et al., 2025). Consistent with these observations, giant-planet thermosphere-ionosphere models show that auroral energy input, Joule heating, ion drag, and rapid rotation can substantially control upper-atmospheric circulation and thermal structure (Achilleos et al., 1998; Bougher et al., 2005; Yates et al., 2020; Müller-Wodarg et al., 2025). Thus, for Jupiter and Saturn, the wind-dynamo pathway isolated here should be viewed as a weak, complementary limiting process rather than an alternative to magnetospheric driving.

Because the simulations use Earth-based planetary parameters, an aligned dipole, Earth-like solar irradiation, and Earth-like lower-boundary forcing while only the Coriolis forcing is scaled, they should be interpreted as controlled reference cases for the stand-alone closed-cap wind dynamo. At Earth, the Pedersen conductivity generally peaks in the E region during the daytime and the lower F region at night. The altitude of this peak is planet dependent, while the overall wind-dynamo response is determined by currents integrated along magnetic field lines rather than by the wind at a single altitude (Richmond, 1995a; Rishbeth, 1997; Heelis, 2004; Chen & Lei, 2019). More generally, the results may be useful for considering weakly forced closed polar caps at gas giants, ice giants, or exoplanets, but quantitative applications will require coupled magnetosphere-ionosphere-thermosphere models with planet-specific magnetic geometry, magnetospheric forcing, realistic lower-atmospheric tidal boundary, and vertically resolved neutral-wind and electrodynamic responses.

Acknowledgments

This work is supported by National Key R&D Program of China (2025YFF0512400). JC is supported by Guangdong Basic and Applied Basic Research Foundation (Grant No. 2026A1515011076). BZ was supported by the Research Grants Council (RGC) Research Fellow Scheme (RFS2526-7S05) and RGC General Research Fund (grant Nos. 17308723, 17309224 and 17309725). We thank Wenbin Wang for his suggestions on numerical experiments.

Data Availability Statement

The model outputs used to reproduce Figures 1–4 in this paper are being preserved online via Chen (2026).

Conflict of Interest

The authors declare no conflicts of interest relevant to this study.

References

Achilleos, N., Miller, S., Tennyson, J., Aylward, A. D., Mueller-Wodarg, I., & Rees, D. (1998). Jim: A Time-Dependent, Three-Dimensional Model of Jupiter's Thermosphere and Ionosphere. *Journal of Geophysical Research: Planets, 103*(E9), 20089-20112. https://doi.org/10.1029/98JE00947

Badman, S. V., & Cowley, S. W. H. (2007). Significance of Dungey-Cycle Flows in Jupiter's and Saturn's Magnetospheres, and Their Identification on Closed Equatorial Field Lines. *Annales Geophysicae, 25*(4), 941-951. https://doi.org/10.5194/angeo-25-941-2007

Bougher, S. W., Waite Jr, J. H., Majeed, T., & Gladstone, G. R. (2005). Jupiter Thermospheric General Circulation Model (Jtgcm): Global Structure and Dynamics Driven by Auroral and Joule Heating. *Journal of Geophysical Research: Planets, 110*(E4). https://doi.org/10.1029/2003JE002230

Bunce, E. J., Arridge, C. S., Clarke, J. T., Coates, A. J., Cowley, S. W. H., Dougherty, M. K., Gérard, J. C., Grodent, D., Hansen, K. C., Nichols, J. D., Southwood, D. J., & Talboys, D. L. (2008). Origin of Saturn's Aurora: Simultaneous Observations by Cassini and the Hubble Space Telescope. *Journal of Geophysical Research: Space Physics, 113*(A9). https://doi.org/10.1029/2008JA013257

Cavalié, T., Benmahi, B., Hue, V., Moreno, R., Lellouch, E., Fouchet, T., Hartogh, P., Rezac, L., Greathouse, T. K., Gladstone, G. R., Sinclair, J. A., Dobrijevic, M., Billebaud, F., & Jarchow, C. (2021). First Direct Measurement of Auroral and Equatorial Jets in the Stratosphere of Jupiter. *A&A, 647*. 10.1051/0004-6361/202140330. https://doi.org/10.1051/0004-6361/202140330

Chaufray, J. Y., Greathouse, T. K., Gladstone, G. R., Waite, J. H., Maillard, J. P., Majeed, T., Bougher, S. W., Lellouch, E., & Drossart, P. (2011). Spectro-Imaging Observations of Jupiter's 2µm Auroral Emission. Ii: Thermospheric Winds. *Icarus, 211*(2), 1233-1241. https://doi.org/10.1016/j.icarus.2010.11.021

Chen, J. (2026). *Data of "Effects of Planetary Rotation on the Ionospheric Electrodynamics with Closed-Field, Magnetospherically Unforced Polar Caps"*. [Dataset] https://doi.org/10.17605/OSF.IO/UBPK3

Chen, J., & Lei, J. (2019). A Simulation Study on the Latitudinal Variations of Ionospheric Zonal Electric Fields under Geomagnetically Quiet Conditions. *Journal of Geophysical Research: Space Physics, 124*(2), 1444-1453. https://doi.org/10.1029/2018ja026174

Chen, J., Zhang, B., Lin, D., Delamere, P. A., Yao, Z., Brambles, O., Sorathia, K. A., Merkin, V. G., & Lyon, J. G. (2023). Prediction of Axial Asymmetry in Jovian Magnetopause Reconnection. *Geophysical Research Letters, 50*(9), e2022GL102577. https://doi.org/10.1029/2022GL102577

Cowley, S. W. H., & Bunce, E. J. (2001). Origin of the Main Auroral Oval in Jupiter's Coupled Magnetosphere–Ionosphere System. *Planetary and Space Science, 49*(10), 1067-1088. https://doi.org/10.1016/S0032-0633(00)00167-7

Cowley, S. W. H., Bunce, E. J., & O'Rourke, J. M. (2004). A Simple Quantitative Model of Plasma Flows and Currents in Saturn's Polar Ionosphere. *Journal of Geophysical Research: Space Physics, 109*(A5). https://doi.org/10.1029/2003JA010375

Cowley, S. W. H., Bunce, E. J., Stallard, T. S., & Miller, S. (2003). Jupiter's Polar Ionospheric Flows: Theoretical Interpretation. *Geophysical Research Letters, 30*(5). https://doi.org/10.1029/2002GL016030

Cowley, S. W. H., & Lockwood, M. (1992). *Excitation and Decay of Solar Wind-Driven Flows in the Magnetosphere-Ionosphere System.* Paper presented at the Annales Geophysicae.

Crary, F. J., Clarke, J. T., Dougherty, M. K., Hanlon, P. G., Hansen, K. C., Steinberg, J. T., Barraclough, B. L., Coates, A. J., Gérard, J. C., Grodent, D., Kurth, W. S., Mitchell, D. G., Rymer, A. M., & Young, D. T. (2005). Solar Wind Dynamic Pressure and Electric Field as the Main Factors Controlling Saturn's Aurorae. *Nature, 433*(7027), 720-722. https://doi.org/10.1038/nature03333

Crooker, N. U., & Rich, F. J. (1993). Lobe Cell Convection as a Summer Phenomenon. *Journal of Geophysical Research: Space Physics, 98*(A8), 13403-13407. https://doi.org/10.1029/93JA01037

Delamere, P. A., & Bagenal, F. (2010). Solar Wind Interaction with Jupiter's Magnetosphere. *Journal of Geophysical Research: Space Physics, 115*(A10). https://doi.org/10.1029/2010JA015347

Delamere, P. A., & Bagenal, F. (2013). Magnetotail Structure of the Giant Magnetospheres: Implications of the Viscous Interaction with the Solar Wind. *Journal of Geophysical Research: Space Physics, 118*(11), 7045-7053. https://doi.org/10.1002/2013JA019179

Dungey, J. W. (1961). Interplanetary Magnetic Field and the Auroral Zones. *Physical Review Letters, 6*(2), 47-48. https://doi.org/10.1103/PhysRevLett.6.47

Foster, J. C., & Rich, F. J. (1998). Prompt Midlatitude Electric Field Effects During Severe Geomagnetic Storms. *Journal of Geophysical Research: Space Physics, 103*(A11), 26367-26372. https://doi.org/10.1029/97JA03057

Giles, R. S., Fletcher, L. N., Irwin, P. G. J., Melin, H., & Stallard, T. S. (2016). Detection of H3+ Auroral Emission in Jupiter’s 5-Micron Window. *A&A, 589*. 10.1051/0004-6361/201628170. https://doi.org/10.1051/0004-6361/201628170

Green, J. A. M., Huber, M., Waltham, D., Buzan, J., & Wells, M. (2017). Explicitly Modelled Deep-Time Tidal Dissipation and Its Implication for Lunar History. *Earth and Planetary Science Letters, 461*, 46-53. https://doi.org/10.1016/j.epsl.2016.12.038

Gurnett, D. A., Kurth, W. S., Hospodarsky, G. B., Persoon, A. M., Zarka, P., Lecacheux, A., Bolton, S. J., Desch, M. D., Farrell, W. M., Kaiser, M. L., Ladreiter, H. P., Rucker, H. O., Galopeau, P., Louarn, P., Young, D. T., Pryor, W. R., & Dougherty, M. K. (2002). Control of Jupiter's Radio Emission and Aurorae by the Solar Wind. *Nature, 415*(6875), 985-987. https://doi.org/10.1038/415985a

Hagan, M. E., & Forbes, J. M. (2002). Migrating and Nonmigrating Diurnal Tides in the Middle and Upper Atmosphere Excited by Tropospheric Latent Heat Release. *Journal of Geophysical Research: Atmospheres, 107*(D24), 4754. https://doi.org/10.1029/2001jd001236

Hagan, M. E., & Forbes, J. M. (2003). Migrating and Nonmigrating Semidiurnal Tides in the Upper Atmosphere Excited by Tropospheric Latent Heat Release. *Journal of Geophysical Research: Space Physics, 108*(A2), 1062. https://doi.org/10.1029/2002ja009466

Heelis, R. A. (2004). Electrodynamics in the Low and Middle Latitude Ionosphere: A Tutorial. *Journal of Atmospheric and Solar-Terrestrial Physics, 66*(10), 825-838. https://doi.org/10.1016/j.jastp.2004.01.034

Heelis, R. A., Lowell, J. K., & Spiro, R. W. (1982). A Model of the High-Latitude Ionospheric Convection Pattern. *Journal of Geophysical Research: Space Physics, 87*(A8), 6339-6345. https://doi.org/10.1029/JA087iA08p06339

Hill, T. W. (1979). Inertial Limit on Corotation. *Journal of Geophysical Research: Space Physics, 84*(A11), 6554-6558. https://doi.org/10.1029/JA084iA11p06554

Johnson, R. E., Stallard, T. S., Melin, H., Nichols, J. D., & Cowley, S. W. H. (2017). Jupiter's Polar Ionospheric Flows: High Resolution Mapping of Spectral Intensity and Line-of-Sight Velocity of H3 + Ions. *Journal of Geophysical Research: Space Physics, 122*(7), 7599-7618. https://doi.org/10.1002/2017JA024176

Kelley, M. C. (2009). *The Earth's Ionosphere: Plasma Physics and Electrodynamics*: Academic press.

Khurana, K. K., Kivelson, M. G., Vasyliunas, V. M., Krupp, N., Woch, J., Lagg, A., Mauk, B. H., & Kurth, W. S. (2004). The Configuration of Jupiter's Magnetosphere. In (Vol. 1, pp. 593-616): Cambridge Univ. Press Cambridge, U. K.

Kivelson, M. G., & Ridley, A. J. (2008). Saturation of the Polar Cap Potential: Inference from Alfvén Wing Arguments. *Journal of Geophysical Research: Space Physics, 113*(A5). https://doi.org/10.1029/2007JA012302

Lu, G., Li, W. H., Raeder, J., Deng, Y., Rich, F., Ober, D., Zhang, Y. L., Paxton, L., Ruohoniemi, J. M., Hairston, M., & Newell, P. (2011). Reversed Two-Cell Convection in the Northern and Southern Hemispheres During Northward Interplanetary Magnetic Field. *Journal of Geophysical Research: Space Physics, 116*(A12). https://doi.org/10.1029/2011JA017043

McComas, D. J., & Bagenal, F. (2007). Jupiter: A Fundamentally Different Magnetospheric Interaction with the Solar Wind. *Geophysical Research Letters, 34*(20). https://doi.org/10.1029/2007GL031078

McComas, D. J., & Bagenal, F. (2008). Reply to Comment by S. W. H. Cowley Et Al. On "Jupiter: A Fundamentally Different Magnetospheric Interaction with the Solar Wind". *Geophysical Research Letters, 35*(10). https://doi.org/10.1029/2008GL034351

Millward, G., Miller, S., Stallard, T., Achilleos, N., & Aylward, A. D. (2005). On the Dynamics of the Jovian Ionosphere and Thermosphere.: Iv. Ion–Neutral Coupling. *Icarus, 173*(1), 200-211. https://doi.org/10.1016/j.icarus.2004.07.027

Mitchell, R. N., & Kirscher, U. (2023). Mid-Proterozoic Day Length Stalled by Tidal Resonance. *Nature Geoscience, 16*(7), 567-569. https://doi.org/10.1038/s41561-023-01202-6

Müller-Wodarg, I. C. F., Iñurrigarro, P., Moore, L., Koskinen, T. T., & Medvedev, A. S. (2025). Temperatures of Jupiter's Upper Atmosphere: The Role of the Planetary Magnetic Field. *The Astrophysical Journal Letters, 990*(1), L22. https://doi.org/10.3847/2041-8213/adfa21

Nichols, J. D. (2011). Magnetosphere-Ionosphere Coupling in Jupiter's Middle Magnetosphere: Computations Including a Self-Consistent Current Sheet Magnetic Field Model. *Journal of Geophysical Research: Space Physics, 116*(A10). https://doi.org/10.1029/2011JA016922

O'Donoghue, J., Moore, L., Bhakyapaibul, T., Melin, H., Stallard, T., Connerney, J. E. P., & Tao, C. (2021). Global Upper-Atmospheric Heating on Jupiter by the Polar Aurorae. *Nature, 596*(7870), 54-57. https://doi.org/10.1038/s41586-021-03706-w

Rasmussen, C. E., & Schunk, R. W. (1987). Ionospheric Convection Driven by Nbz Currents. *Journal of Geophysical Research: Space Physics, 92*(A5), 4491-4504. https://doi.org/10.1029/JA092iA05p04491

Rego, D., Achilleos, N., Stallard, T., Miller, S., Prangé, R., Dougherty, M., & Joseph, R. D. (1999). Supersonic Winds in Jupiter's Aurorae. *Nature, 399*(6732), 121-124. https://doi.org/10.1038/20121

Reiff, P. H., & Heelis, R. A. (1994). Four Cells or Two? Are Four Convection Cells Really Necessary? *Journal of Geophysical Research: Space Physics, 99*(A3), 3955-3959. https://doi.org/10.1029/93JA01992

Richmond, A. D. (1995a). *Ionospheric Electrodynamics* (Vol. 1): CRC Press.

Richmond, A. D. (1995b). Ionospheric Electrodynamics Using Magnetic Apex Coordinates. *Journal of geomagnetism and geoelectricity, 47*(2), 191-212. https://doi.org/10.5636/jgg.47.191

Richmond, A. D., & Maute, A. (2014). Ionospheric Electrodynamics Modeling. *Modeling the Ionosphere–Thermosphere System*, 57-71. https://doi.org/10.1002/9781118704417.ch6

Richmond, A. D., Ridley, E. C., & Roble, R. G. (1992). A Thermosphere/Ionosphere General Circulation Model with Coupled Electrodynamics. *Geophysical Research Letters, 19*(6), 601-604. https://doi.org/10.1029/92GL00401

Richmond, A. D., & Roble, R. G. (1987). Electrodynamic Effects of Thermospheric Winds from the Ncar Thermospheric General Circulation Model. *Journal of Geophysical Research: Space Physics, 92*(A11), 12365-12376. https://doi.org/10.1029/JA092iA11p12365

Richmond, A. D., & Thayer, J. P. (2000). Ionospheric Electrodynamics: A Tutorial. *Geophysical Monograph Series, 118*, 131.

Rishbeth, H. (1997). The Ionospheric E-Layer and F-Layer Dynamos — a Tutorial Review. *Journal of Atmospheric and Solar-Terrestrial Physics, 59*(15), 1873-1880. https://doi.org/10.1016/S1364-6826(97)00005-9

Roble, R. G., Ridley, E. C., Richmond, A. D., & Dickinson, R. E. (1988). A Coupled Thermosphere/Ionosphere General Circulation Model. *Geophysical Research Letters, 15*(12), 1325-1328. https://doi.org/10.1029/GL015i012p01325

Ruohoniemi, J. M., & Greenwald, R. A. (2005). Dependencies of High-Latitude Plasma Convection: Consideration of Interplanetary Magnetic Field, Seasonal, and Universal Time Factors in Statistical Patterns. *Journal of Geophysical Research: Space Physics, 110*(A9). https://doi.org/10.1029/2004JA010815

Schunk, R. W., & Nagy, A. F. (2000). *Ionospheres: Physics, Plasma Physics, and Chemistry*: Cambridge university press.

Stallard, T. S., Miller, S., Cowley, S. W. H., & Bunce, E. J. (2003). Jupiter's Polar Ionospheric Flows: Measured Intensity and Velocity Variations Poleward of the Main Auroral Oval. *Geophysical Research Letters, 30*(5). https://doi.org/10.1029/2002GL016031

Stallard, T. S., Miller, S., & Melin, H. (2012). Clues on Ionospheric Electrodynamics from Ir Aurora at Jupiter and Saturn. *Auroral phenomenology and magnetospheric processes: Earth and other planets, 197*, 215-224.

Stallard, T. S., Miller, S., Melin, H., Lystrup, M., Dougherty, M., & Achilleos, N. (2007a). Saturn's Auroral/Polar H+3 Infrared Emission: I. General Morphology and Ion Velocity Structure. *Icarus, 189*(1), 1-13. https://doi.org/10.1016/j.icarus.2006.12.027

Stallard, T. S., Miller, S., Millward, G., & Joseph, R. D. (2001). On the Dynamics of the Jovian Ionosphere and Thermosphere: I. The Measurement of Ion Winds. *Icarus, 154*(2), 475-491. https://doi.org/10.1006/icar.2001.6681

Stallard, T. S., Smith, C., Miller, S., Melin, H., Lystrup, M., Aylward, A., Achilleos, N., & Dougherty, M. (2007b). Saturn's Auroral/Polar H+3 Infrared Emission: Ii. A Comparison with Plasma Flow Models. *Icarus, 191*(2), 678-690. https://doi.org/10.1016/j.icarus.2007.05.016

Szalay, J. R., Clark, G., Livadiotis, G., McComas, D. J., Mitchell, D. G., Rankin, J. S., Sulaiman, A. H., Allegrini, F., Bagenal, F., Ebert, R. W., Gladstone, G. R., Kurth, W. S., Mauk, B. H., Valek, P. W., Wilson, R. J., & Bolton, S. J. (2022). Closed Fluxtubes and Dispersive Proton Conics at Jupiter's Polar Cap. *Geophysical Research Letters, 49*(9), e2022GL098741. https://doi.org/10.1029/2022GL098741

Tan, Y., Dang, T., Lei, J., Zhang, B., Wang, W., Yang, Z., Pham, K., & Sorathia, K. (2022). Interplanetary Control of High-Latitude Thermospheric Winds: Results from Hiwind and Model Simulations. *Journal of Geophysical Research: Space Physics, 127*(9), e2022JA030394. https://doi.org/10.1029/2022JA030394

Tao, C., Badman, S. V., & Fujimoto, M. (2011). Uv and Ir Auroral Emission Model for the Outer Planets: Jupiter and Saturn Comparison. *Icarus, 213*(2), 581-592. https://doi.org/10.1016/j.icarus.2011.04.001

Tarbuck, E. J., & Lutgens, F. K. (1979). *The Atmosphere: An Introduction to Meteorology*: Prentice Hall.

Thayer, J. P., & Vickrey, J. F. (1992). On the Contribution of the Thermospheric Neutral Wind to High-Latitude Energetics. *Geophysical Research Letters, 19*(3), 265-268. https://doi.org/10.1029/91GL02868

Tsubota, T. K., Wong, M. H., Stallard, T., Zhang, X., & Simon, A. A. (2025). Uv-Dark Polar Ovals on Jupiter as Tracers of Magnetosphere–Atmosphere Connections. *Nature Astronomy, 9*(2), 221-229. https://doi.org/10.1038/s41550-024-02419-0

Wang, R., Stallard, T. S., Melin, H., Baines, K. H., Achilleos, N., Rymer, A. M., Ray, L. C., Nichols, J. D., Moore, L., O'Donoghue, J., Chowdhury, M. N., Thomas, E. M., Knowles, K. L., Tiranti, P. I., & Miller, S. (2023). Asymmetric Ionospheric Jets in Jupiter's Aurora. *Journal of Geophysical Research: Space Physics, 128*(12), e2023JA031861. https://doi.org/10.1029/2023JA031861

Wang, W., Burns, A. G., Wiltberger, M., Solomon, S. C., & Killeen, T. L. (2008a). Altitude Variations of the Horizontal Thermospheric Winds During Geomagnetic Storms. *Journal of Geophysical Research: Space Physics, 113*(A2), A02301. https://doi.org/10.1029/2007ja012374

Wang, W., Lei, J., Burns, A. G., Wiltberger, M., Richmond, A. D., Solomon, S. C., Killeen, T. L., Talaat, E. R., & Anderson, D. N. (2008b). Ionospheric Electric Field Variations During a Geomagnetic Storm Simulated by a Coupled Magnetosphere Ionosphere Thermosphere (Cmit) Model. *Geophysical Research Letters, 35*(18), L18105. https://doi.org/10.1029/2008GL035155

Weimer, D. R. (2005). Improved Ionospheric Electrodynamic Models and Application to Calculating Joule Heating Rates. *Journal of Geophysical Research: Space Physics, 110*(A5), A05306. https://doi.org/10.1029/2004JA010884

Xu, J., Smith, A. K., Wang, W., Jiang, G., Yuan, W., Gao, H., Yue, J., Funke, B., López-Puertas, M., & Russell Iii, J. M. (2013). An Observational and Theoretical Study of the Longitudinal Variation in Neutral Temperature Induced by Aurora Heating in the Lower Thermosphere. *Journal of Geophysical Research: Space Physics, 118*(11), 7410-7425. https://doi.org/10.1002/2013JA019144

Yates, J. N., Ray, L. C., Achilleos, N., Witasse, O., & Altobelli, N. (2020). Magnetosphere-Ionosphere-Thermosphere Coupling at Jupiter Using a Three-Dimensional Atmospheric General Circulation Model. *Journal of Geophysical Research: Space Physics, 125*(1), e2019JA026792. https://doi.org/10.1029/2019JA026792

Zhang, B., Delamere, P. A., Yao, Z., Bonfond, B., Lin, D., Sorathia, K. A., Brambles, O. J., Lotko, W., Garretson, J. S., Merkin, V. G., Grodent, D., Dunn, W. R., & Lyon, J. G. (2021). How Jupiter's Unusual Magnetospheric Topology Structures Its Aurora. *Science Advances, 7*(15), eabd1204. https://doi.org/10.1126/sciadv.abd1204

Zhang, B., Yao, Z., Brambles, O. J., Delamere, P. A., Lotko, W., Grodent, D., Bonfond, B., Chen, J., Sorathia, K. A., Merkin, V. G., & Lyon, J. G. (2024). A Unified Framework for Global Auroral Morphologies of Different Planets. *Nature Astronomy, 8*, 964–972. https://doi.org/10.1038/s41550-024-02270-3